Engineering Structures 234 (2021) 111969

Contents lists available at ScienceDirect

Engineering Structures

journal homepage: www.elsevier.com/locate/engstruct

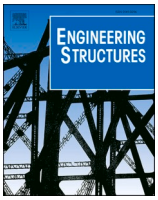

Flexural strengthening of RC beams using aluminum alloy plates with mechanically-fastened anchorage systems: An experimental investigation

Omar R. Abuodeh [a,*], Jamal A. Abdalla [b], Rami A. Hawileh [b]

[a] Department of Civil Engineering, Clemson University, Clemson, SC 29634, USA
[b] Department of Civil Engineering, American University of Sharjah, United Arab Emirates

ARTICLE INFO

Keywords:
Flexural strengthening
Aluminum alloy plates
Mechanical fasteners
Expansion anchor bolts
Anchorage systems
Externally bonded reinforcement
Ductility
Reinforced concrete beams

ABSTRACT

Externally bonded reinforcement (EBR) has emerged as one of the promising techniques for flexural strengthening of reinforced concrete (RC) members due to its practicality and structural effectiveness. However, shortcomings like premature failure modes, cost, labor, and installation time limited its use. Mechanically fastened (MF) Aluminum Alloy (AA) plates instead have the potential to overcome some of these drawbacks by providing strength and ductility, while influencing the failure modes. In this investigation, 16 RC beams were prepared, one beam was left un-strengthened (CB), one was strengthened with an externally bonded (EB) AA plate (CBE), and the remaining 14 beams were strengthened with MF AA plates that varied based on expansion anchor bolts (EAB) sizes, spacing, layout, and the presence or absence of epoxy. The test results indicated that all the specimens with MF AA plates exhibited approximately 30% increase in strength accompanied with drastic increase in ductility up to about 84% compared to specimen CBE. Analytical predictions were made to numerically assess the advantages of using MF systems where ACI 318-19 outperformed ACI 440.2R-17 due to the sufficient composite behavior that allows the AA plates to behave similar to steel reinforcement such that the section has an additional lever arm. It is concluded that the implementation of epoxy and EAB as an alternative anchorage technique serves as a viable approach in enhancing the strength and ductility of RC beams strengthened with AA plates.

1. Introduction

A significant number of high-rise buildings were constructed during the first half of the 20th century using reinforced concrete (RC), precast and steel construction materials. Recently, most of these buildings have begun showing signs of deterioration in the form of steel corrosion and concrete cracking/spalling [1]. This advocated researchers and engineers to implement strengthening strategies, which involved externally bonding composite materials on the surfaces of damaged structural members [2-4]. In particular, an underlying topic that has been under rigorous research is flexural strengthening of RC beams under monotonic and cyclic loading [5-8]. The main concept of flexural strengthening applications is bonding the composite material to the RC beam's soffit such that an additional lever arm is introduced to the section, supplementing it with a larger moment capacity [9]. Several studies were conducted in which the strength gain of RC beams ranged from 40% to 220% compared to that of un-strengthened RC beams using aluminum alloy (AA) plates, hard-wire steel mesh, stainless steel, and fiber-reinforce polymers (FRP) composites [10-14].

This strengthening application is often susceptible to premature failure due to delamination (concrete cover separation) or debonding of the externally bonded reinforcement (EBR) composite materials [15]. Moreover, EBR applications involve intensive labor costs due to the time consumed in surface preparations, adhesive mixing and placing [16]. Therefore, researchers investigated unique anchorage techniques that would mitigate these failure modes and enhance the RC specimen's load-carrying capacity without completely hindering its ductility [17]. These techniques include using FRP wraps along with the EBR composite materials [18], installed FRP splay anchors via drilled holes along the EBR composite materials [5], and mechanically fastened (MF) EBR composite materials [15]. These anchorage systems changed the failure modes from debonding/delamination to either local debonding at locations within the vicinity of loading plates [5,16] or composite plate rupture without exhibiting any plastic hardening [15]. Either failure mode demonstrates no sign of plastic softening, which could help in warning engineers prior to failure.

A series of experimental and numerical investigations on using high strength AA plates as an EBR for RC beams have been conducted by

* Corresponding author.
E-mail addresses: oabuode@g.clemson.edu (O.R. Abuodeh), jabdalla@aus.edu (J.A. Abdalla), rhaweeleh@aus.edu (R.A. Hawileh).

https://doi.org/10.1016/j.engstruct.2021.111969
Received 19 May 2020; Received in revised form 20 January 2021; Accepted 24 January 2021
Available online 13 February 2021

many researchers [11,19-23]. The desired characteristics of high strength AA plates such as high ductility compared to that of FRP, lightweight compared to that of stainless steel and ordinary steel, and high resistance to corrosion compared to both steel and FRP, respectively, made it a strong candidate as an EBR material. Rasheed et al. [11] conducted an experiment on using AA plates with/without single-layer and double-layer U-wrapped CFRP sheets in externally strengthening RC beams in flexure. Their test program included a group of RC beams, where some of them were strengthened using externally bonded (EB) AA plates with different FRP U-wraps as end-anchors and spaced throughout the specimens. The results were compared to a control un-strengthened specimen. It was observed that the strengthened beams had an increase in strength from 13 to 40% and an increase in deflection from 2.31 to 42.7% when compared to the un-strengthened specimen. This made AA plates a viable option in applications involving efficient anchorage techniques for strengthened RC beams to exhibit significant yielding, as a sign of warning, prior to failure.

The use of MF composite materials, in particular, has received a lot of attention in flexural strengthening applications [15,16,22,24]. MF strengthened systems are prepared by *bolting* composite plates to concrete members without any adhesive bonding or surface preparation; resulting in significant savings in terms of cost, labor and time [15]. These anchorage systems have demonstrated promising results in terms of providing sufficient loading capacity while maintaining the structural member's ductility. The common failure modes associated with MF systems are dependent on the type of anchors used. For example, El-Meddawy et al. [15] has tested the implementation of MF-FRP systems using expansion anchor bolts (EAB), threaded anchor bolts (TAB), and powder-actuated fasteners (PAF). It was reported that the retrofitted specimens that were MF with EAB and TAB were more effective in improving the flexural capacity of RC beams compared with the specimens that were MF with PAF. In particular, the EAB fastening system demonstrated significant ductility when compared to the strengthened specimens MF with TAB and PAF, respectively. Moreover, the failure modes of the RC beams that were MF with EAB consisted of a combination of concrete crushing with steel yielding until local bearing failure occurred on the FRP plates around the EAB. This indicated that much of the composite material's mechanical properties were utilized during all stages of loading.

This paper aims to study the effects of using MF and EB anchorage systems on the flexural strength, stiffness, and ductility RC beams externally strengthened with AA plates. In this study, sixteen RC beams were prepared, where one beam was left un-strengthened, one beam was externally strengthened using an EB AA plate, seven beams were strengthened using MF and EB AA plates, and the remaining seven beams were externally strengthened with only MF AA plates. In addition, the test results were predicted using the ACI 318-19 [25] and ACI 440.2R-17 [9].

2. Experimental program

A total of 16 RC beams were designed to fail in flexure in accordance with the ACI 318-19 [25] design provisions. The dimension of each specimen was 1840 mm × 240 mm × 125 mm in length, height, and width, respectively. The longitudinal reinforcing bottom and top steel bar diameters used were 10 mm and 8 mm, respectively, and the transverse reinforcement (stirrups) were 8 mm in diameter and spaced at 100 mm center-to-center. Fig. 1 shows the dimensions of the cast RC beams together with its longitudinal and transverse reinforcement detailing. A summary of the test matrix is shown in Table 1.

The experimental program was divided into three groups of specimens; control beam group (CBG), a group strengthened and anchored with 10 mm diameter steel EAB (M10), and a group anchored with 12 mm diameter steel EAB (M12). The CBG consisted of two specimens; namely, an un-strengthened beam (CB) shown in Fig. 1 and a beam strengthened with an externally epoxy-bonded AA plate (CBE) shown in Fig. 2. Both specimens served as benchmarks for comparison with the strengthened beams that were MF with EB or without EB anchorage systems.

The M10 and M12 groups of specimens were designated depending on the EAB diameter, embedment depth, torque magnitude, and layout. In this study, two types of EAB were used; namely, HST3-M10 × 90 and HST3-M12 × 110, which were provided by the manufacturer [26]. Table 1 presents the test program followed in this study where the prefixes "B","BE", "M10H", "M10L", "M10E", "M12H", "M12L", "M12E" refer to "beam without epoxy", "beam with epoxy", "high number of HST3-M10 EAB", "low number of HST3-M10 EAB", "HST3-M10 EAB anchored at the edge of the plates", "high number of HST3-M12 EAB", "low number of HST3-M12 EAB", and "HST3-M12 EAB anchored at the edge of the plates". For example, specimen BEM10H designates a beam strengthened with AA plates using epoxy and high number of HST3-M10 EAB. Fig. 3 shows the geometric properties of the specimens in M10 and M12 groups where the total reinforcing ratio is 1.024% (i.e. the sum total of the reinforcing ratios for both the internal and external reinforcements). It is worth mentioning that EAB installation should be used in light-to-medium reinforced sections since the internal longitudinal and transverse reinforcement could interfere with anchor positioning. Further description related to the material's mechanical properties will be discussed in the following sections.

2.1. Material specification

In this study, the materials used were normal weight concrete, normal strength deformed steel bars, and 3 mm thick Aluminum Alloy AA5083-H111 plates. Their mechanical properties were obtained by conducting compressive and tensile tests as per ASTM standards [27-29]. Concrete cubes/cylinders and steel coupons were prepared in the lab and tested accordingly. As a result, four 150 mm × 150 mm × 150 mm cubes as per [BS 1881, Part 108: 1993] where their average compressive strength, standard deviation, and coefficient of variation was 46.25 MPa, 1.5 MPa, and 3.24%, respectively. The concrete cylinder compressive strength was estimated as 0.8 multiplied by the average compressive strength in cubes, as per [BS 1881, Part 108: 1993], to be used in the numerical predictions of the tested specimens. In addition,

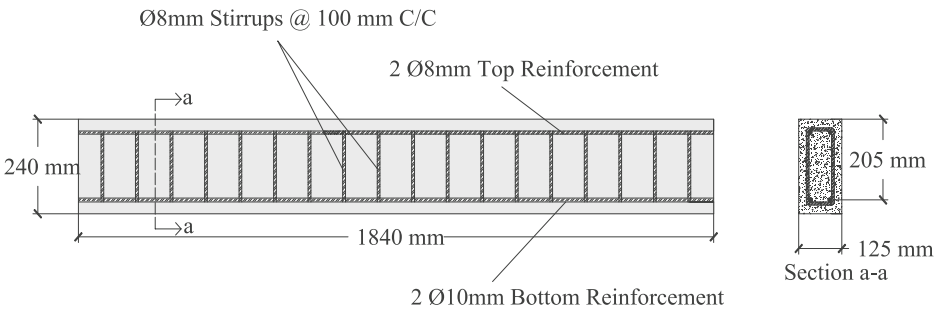

Fig. 1. Geometric and reinforcement detailing for all RC beams.

Table 1
Test matrix.

Specimen Designation	Anchorage		EAB details			EAB layout		
	Epoxy	EAB	Spacing (mm)	Diameter (mm)	Embedment Depth (mm)	Series	Edge	Number of beams
CB	–	–	–	–	–	–	–	1
CBE	✓	–	–	–	–	–	–	1
BEM10H	✓	✓	100	10	65	✓	–	2
BEM10L	✓	✓	200	10	65	✓	–	2
BEM12H	✓	✓	100	12	80	✓	–	2
BEM12L	✓	✓	200	12	80	✓	–	2
BM10H	–	✓	100	10	65	✓	–	2
BM12H	–	✓	100	12	80	✓	–	2
BEM10E	✓	✓	100	10	65	–	✓	1
BEM12E	✓	✓	100	12	80	–	✓	1

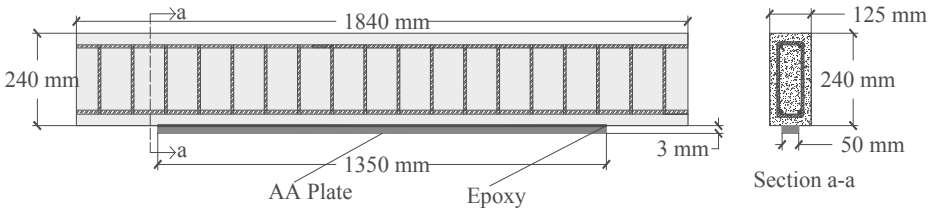

Fig. 2. Dimensions and strengthening scheme of RC CBE specimen.

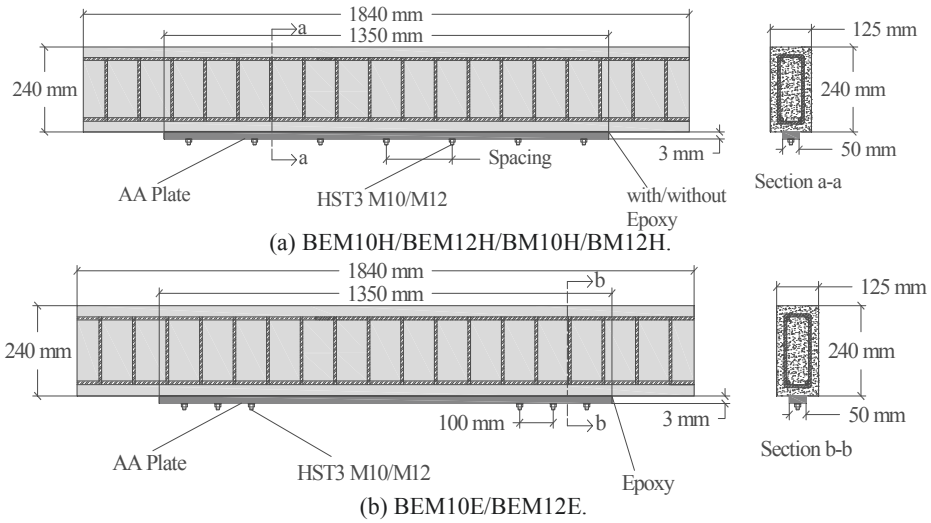

Fig. 3. Dimensions and strengthening scheme of RC beams of M10 and M12 group of specimens.

three tensile tests were conducted for each steel bar size (8 mm and 10 mm) such that stress-strain properties like yield and tensile strengths were obtained to evaluate the elastic modulus. For the Ø8 mm steel bars, the average, standard deviation, and coefficient of variation was: 556.5 MPa, 17.5 MPa, and 3.12%, respectively, for the yield strength, 640.4 MPa, 12.1 MPa, and 1.89%, respectively, for the tensile strength, and 199.9 GPa, 0.10 GPa, and 0.05%, respectively, for the elastic modulus. For the Ø10 mm steel bars, the average, standard deviation, and coefficient of variation was: 548.9 MPa, 8.94 MPa, and 1.63%, respectively, for the yield strength, 645.1 MPa, 12.0 MPa, and 1.86%, respectively, for the tensile strength, and 200.03 GPa, 0.208 GPa, and 0.104%, respectively, for the elastic modulus.

The AA plates were cut into five dog-bone shaped coupons, as per ASTM E8 [29], where the total length, gage length, and grip length were 375 mm, 225 mm and 75 mm, respectively, as shown in Fig. 4. The test setup was carried out by gripping a length of 75 mm from both edges of each AA coupon as shown in Fig. 5**(a)**, and tested using a displacement rate of 0.5 mm/min [29]. As a result, the AA specimens failed by rupture

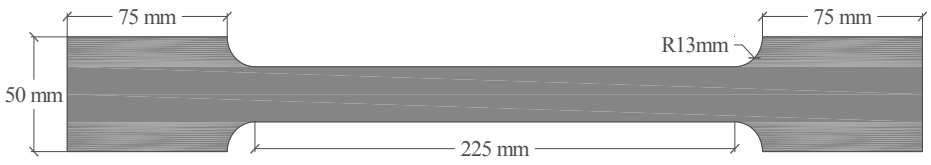

Fig. 4. Dimensions of a Dog-Bone Shaped AA Plate.

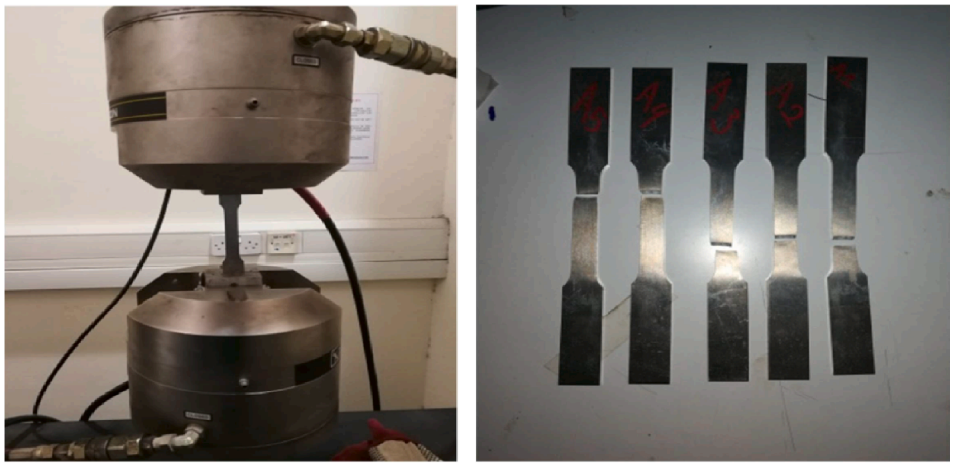

(a) Test setup. (b) Ruptured coupons.

Fig. 5. AA Plate Tensile Test.

within the gage length as shown in Fig. 5**(b)**. Stress versus strain curves were generated, as shown in Fig. 6. The mechanical properties in terms of the yield strength, tensile strength, elastic modulus, and elongation values were computed. Table 2 provides the yield strength (F_y), tensile strength (F_u), elastic modulus (E), and elongation values obtained from the test and manufacturer. It is worth noting that the yield strength and elastic modulus values measured were less than the nominal values prescribed by the manufacturer. This can be attributed to the difference in testing equipment, strain measurements, and sizing of specimens. Nevertheless, the Mean Absolute Error for the yield strength and elastic modulus was 7.50% and 5.00%, which were considered accepted for the scope of this study. Since the stress strain curves of the AA plate do not demonstrate a clear yield point, the 0.2% offset method was used to define the yield strength and thus calculate the elastic modulus, as per ASTM E8 [29]. Other properties like chemical composition and physical properties of the AA plate are presented in Table 3.

The epoxy adhesive's mechanical properties was provided by the manufacturer [31] and reported as 80 MPa, 40 MPa, 8000 MPa, 4000 MPa and 30 MPa for the compressive strength, flexural strength, modulus of elasticity under compression, modulus of elasticity in flexural, and tensile strength, respectively. The geometric properties, mechanical properties, and setting details of HST3-M10 × 90 and HST3-M12 × 105 bolts were obtained from the manufacturer's technical datasheets [26], and are listed in Table 4. Fig. 7 shows the EAB that were

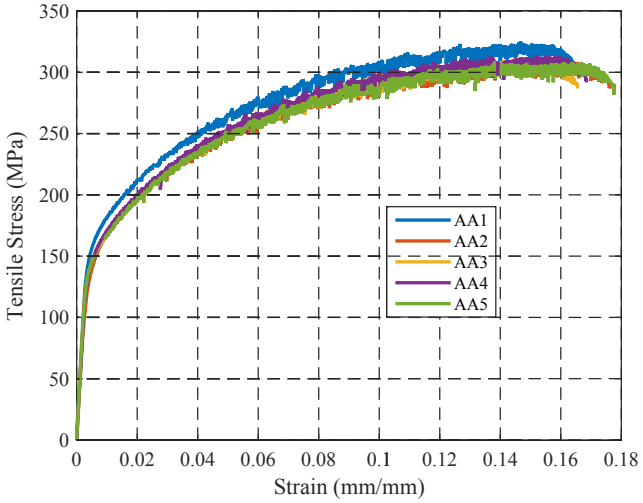

Fig. 6. Stress versus strain curves for AA coupons.

Table 2
AA coupon mechanical properties obtained from the test and manufacturer.

	F_y (MPa)	F_u (MPa)	E (GPa)	Elongation (%)
AA1	161.4	329.2	70.3	16.6
AA2	152.2	319.1	69.8	17.6
AA3	151.7	312.1	69.2	16.5
AA4	148.0	313.5	71.3	17.0
AA5	145.0	309.1	70.9	18.0
Average	151.6	316.6	70.3	17.1
Specifications	163.9	301.5	70.0	21.1
Absolute Percent Difference (%)	7.50	5.00	0.429	18.9

Table 3
Chemical composition and physical properties of 5083-H111 AA [30].

Chemical Properties		Physical and Mechanical Properties	
Chemical element	% Present	Property	Value
Aluminum, Al	93.9%	Density	2.65 g/cm^3
Chromium, Cr	0.05–0.25%	Melting Point	570 °C
Copper, Cu	0.10%	Thermal Expansion	25 × 10^{-6}/K
Iron, Fe	0.40%	Modulus of Elasticity	72 GPa
Magnesium, Mg	4.0–4.9%	Thermal Conductivity	121 W/m.K
Manganese, Mn	0.40–1.00%	Electrical Resistivity	0.058 × 10^{-6} Ω.m
Other (each)	0.0–0.05%	Density	2.65 g/cm^3
Other (total)	0.0–0.15%	Proof Stress	125 Min MPa
Silicon, Si	0.0–0.40%	Tensile Strength	275–350 MPa
Titanium, Ti	0.05–0.25%	Elongation A50 mm	23%
Zinc, Zn	0.108%	Shear Strength	175 MPa
–	–	Hardness Brinee	75 HB

used during this study, where each anchor consists of a nut and a washer. A brief summary of the mechanical properties of the different materials used in this study are presented in Table 5, where f'_c is the average concrete compressive strength, E_c is the average concrete elastic modulus, f_y is the average yield strength of steel, E_s is the average elastic modulus of steel, E_{AA} is the average elastic modulus of the AA plates, ε_{AA} is the strain corresponding to the ultimate strength of the AA plates, $f_{t,AA}$ is the average ultimate strength of the AA plates, E_E is the elastic modulus of epoxy, and $f_{t,E}$ is the tensile strength of epoxy.

2.2. Specimen preparation

Prior to external strengthening, the surfaces of the concrete specimens and AA plates were roughened using an electrical grinder. This

Table 4
EAB manufacturer details [26].

Details[a]	HST3-M10 × 90	HST3-M12 × 105
f_{uta} (MPa)	800	800
$A_{se,V}$ (mm^2)	58	84.3
d_o (mm)	10	12
d_a (mm)	12	14
h_{eff} (mm)	90	105
S_{min} (mm)	70	80
C_{min} (mm)	70	80
T (N-m)	45	60

[a] f_{uta}: tensile strength; $A_{se,V}$ = area of EAB sleeve; d_o = diameter of EAB; d_a = hole diameter according to the manufacturer's instructions [26]; h_{eff} = length of EAB; S_{min} = minimum center-to-center spacing between EAB; C_{min} = minimum distance from EAB to edge of beam; T = torque required to fix EAB.

enhanced the bond behavior between the epoxy and the strengthened system; yielding an ideal surface profile for a more efficient load transfer. In this study, two surface preparation techniques were carried out: mainly, concrete and AA plate surface preparations. During the concrete surface preparation, the beams were flipped to provide access to the soffit of the beam. Afterwards, an electrical grinder was used to abrade the RC beams' soffits until the aggregates were visible as per ACI-546 [32] guidelines. Any loose or dust particles were removed using a pressurized air blower. For AA plates, the surface preparation was carried out by grinding only one side of the AA plates that is facing the soffit of the strengthened beam. This approach of roughening AA surface proved its effectiveness in previous studies [11,21,23].

Once the surface was prepared for each specimen, the locations of the anchors were marked on the AA plates and on the RC beams based on their locations as shown on the schematics shown in Fig. 3. Predrilling was carried out using a rotary hammer drill until the embedment depths outlined in Table 4 were reached. To avoid excessive damage on the concrete specimens and AA plates, two types of drill bits were used; mainly, concrete and steel (for the AA plates) drill bits. Any entrapped dust particles were removed using a pressurized air blower to ease the setting of the EAB and enhance the contact between the sleeves of the EAB and the inner surfaces of the predrilled holes. Afterwards, HST3 M10 × 90 and HST3 M12 × 110 EAB were carefully driven into the holes using a hammer to begin fastening the AA plates. It is worth mentioning that the installation of bolts was conducted such that the bolts did not interfere with the internal steel reinforcement so that galvanic corrosion is prevented. The bonding application was carried out by priming epoxy resin layers according to the manufacturer's specifications [31] in which the resin (part A) and hardener (part B) were mixed with a ratio of 3:1, until the mixture had a uniform grey color.

For the specimens involving both a MF and EB anchorage system, the epoxy was applied within the boundary of the grinded surface, on the soffit of each RC beam, followed by placing the AA plate onto the beam and anchoring the plates with the EAB. On the other hand, the specimens that only consisted of MF anchorage systems had the plates fixed to the EAB without any epoxy bonding. The AA plates were secured into place by using nuts and washers where a specified torque was used for each EAB type, as shown in Table 4, to allow the anchors' sleeves expand outwards. Fig. 8 shows the prepared strengthened specimens that were tested during this study.

2.3. Test setup and instrumentation

A Universal Testing Machine (UTM) was used to test all the RC beams in which a displacement control protocol was followed during the test. The loading rate employed was 2 mm/min, similar to previous experimental investigations [11,21]. All RC beams were loaded using a four-point bending setup with an effective span and shear span lengths of 1740 mm and 600 mm, respectively, as shown in Fig. 9. The aim of this experiment was to monitor the flexural capacity and ductility of each beam at maximum bending; within the vicinity of the loading plates. Therefore, strain and vertical displacement measurements were recorded at mid-span of each beam. For strain measurements, strain gauges were bonded to the concrete surface, bottom flexural steel bars, and AA plate at the mid-span of the RC beams, respectively. For vertical displacement measurements, the UTM machine features a built-in

(a) HST3 M10×90. (b) HST3 M12×110.

Fig. 7. EAB used in MF specimens.

Table 5
Summary of mechanical properties of materials.

Concrete		Steel		AA5038-H111			Epoxy	
f'_c (MPa)	E_c (GPa)	f_y (MPa)	E_s (GPa)	E_{AA} (GPa)	ε_{AA} (%)	$f_{t,AA}$ (MPa)	E_E (GPa)	$f_{t,E}$ (MPa)
36	28.7	550	200	70	17.1	316.6	10	30

(a) BEM10E/BEM12E.

(b) BEM10H/BEM12H.

(c) BEM10L/BEM12L.

(d) BM10H/BM12H.

(e) CBE.

Fig. 8. Bottom view of all retrofitted RC beams.

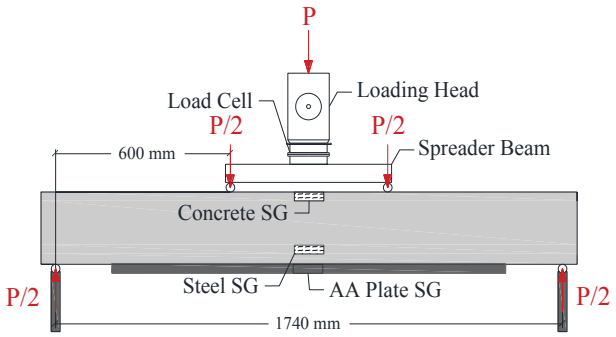

Fig. 9. Load setup and strain gauge placement for all the RC specimens.

electronic displacement transducer that records the position of loading during all stages of loading.

3. Summary of results and discussion

The load-deflection and load-strain relationships for all tested specimens were evaluated to describe and explain the beams' behavior. Emphasis was made on the ductility and failure mode of each specimen to quantify the effect of varying the MF and/or EB anchorage systems on the AA plated RC beams. For brevity, the parameters reported hereafter were: ultimate load (P_u), deflection at ultimate load (Δ_u), deflection at yield load (Δ_y), deflection at failure load (Δ_f), ductility index at failure load ($\delta_f = \Delta_f/\Delta_y$), and ductility index at ultimate load ($\delta_u = \Delta_u/\Delta_y$). All tests were terminated when the load dropped below 20% of the ultimate load.

3.1. Load-deflection response and failure modes

The load versus mid-span deflection curves were plotted for the a selected number of tested specimens as representative, shown in Fig. 10. The specimens in CBG were included to serve as benchmarks for the specimens in both M10 and M12 groups of specimens. All the strengthened beams have shown an increase in strength that ranged between 15.9 and 34.7% compared to CB, irrespective of the type of anchorage system implemented. Furthermore, the incorporation of MF composite systems postponed end-plate debonding (EPD), as depicted in Fig. 11**(a)**. This resulted in plate rupture (PR) or local-plate debonding (LPD), as shown in Fig. 11**(b)–(d)**, and allowed the strengthened specimens to fully utilize the properties of the AA plates. It is worth mentioning that the plate rupture observed was the result of net-tension failure only, as shown in Fig. 11**(b) and (d)**. Furthermore, the installation of bolts would result in significant increase in the beam's capacity and ductility. However, the presence of wider crack widths around the vicinity of the bolted segments is expected as shown in Fig. 11, due to the initiation of crack from the bolt hole. This would thus increase the susceptibility of reinforcement to corrosion in humid or marine environment.

Failure modes like shearing of bolts and bearing on plates have not been visually observed. This is directly related to the mechanical

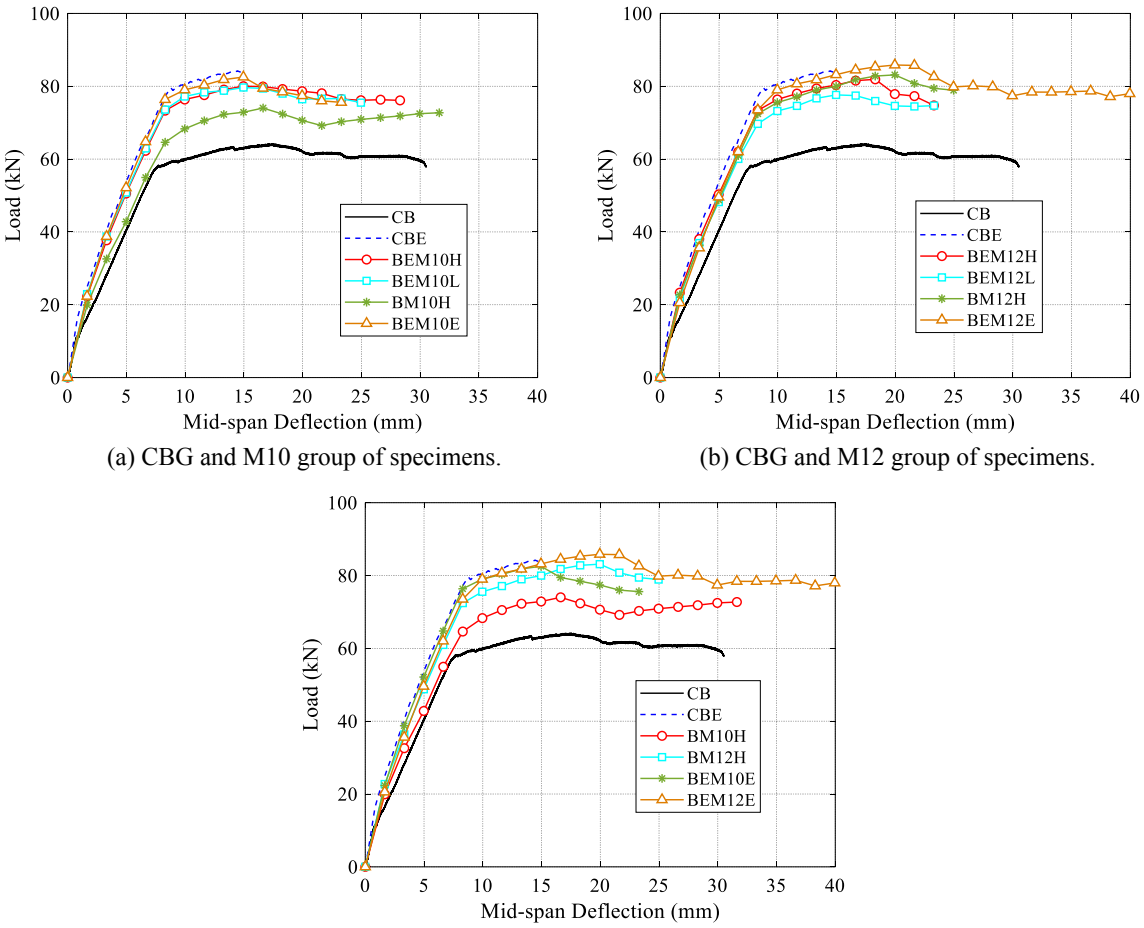

(a) CBG and M10 group of specimens.

(b) CBG and M12 group of specimens.

(c) CB, CBE and selected specimens of M10 and M12 groups.

(d)

Fig. 10. Load versus mid-span deflection curves responses of tested specimens.

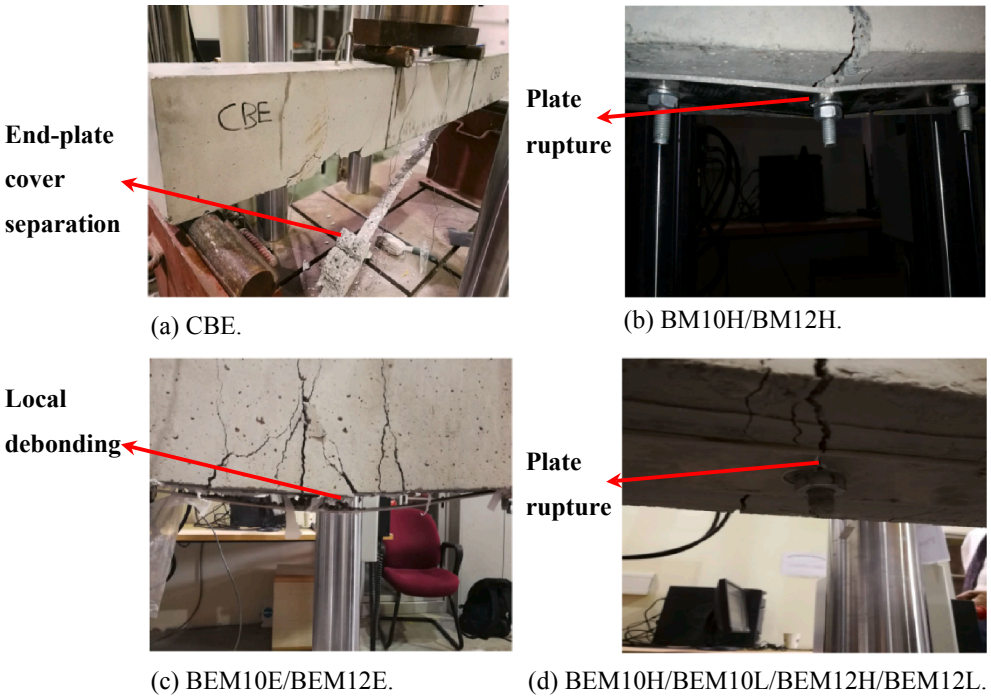

(a) CBE.

(b) BM10H/BM12H.

(c) BEM10E/BEM12E.

(d) BEM10H/BEM10L/BEM12H/BEM12L.

Fig. 11. Failure modes of selected retrofitted RC beams.

properties of the EAB compared to the AA plates, which in this study was at least three times higher than that of the plate. In addition, since a local bearing failure would normally be observed at the end of the plates wherein flexural stresses are lower in simply supported beams [15], local bearing failures did not influence the flexural capacity of the plated RC specimens. Therefore, the shear and bearing capacities of the composite system were not emphasized in the scope of this study. Among the tested specimens, BEM12E showed the best flexural performance in terms of load-carrying capabilities and ductility. Specimens BEM10H, BEM10L, BEM12H and BEM12L, all showed strength gains that ranged between 33.6 and 34.7%. Therefore, increasing the number of anchors and changing from HST3 M10 to M12 anchors did not have any significant effect on the strength gain in the retrofitted specimens with EB AA plates. BM10H and BM12H specimens, however, have demonstrated differences in strength gains, where BM10H and BM12H achieved 15.9% and 30.5%, respectively. This indicated that using EAB with larger diameters, embedment depths, and torque magnitudes provided a more efficient composite action, yielded higher strength gains, and eliminated the necessity of using an adhesive bond within the anchorage system.

The ductility was also an important parameter that was studied in this experimental investigation. To quantify the amount of ductility gained by the strengthened specimens, the deflection of CBE was taken as a benchmark since this study focuses on the effects of using EAB in fastening AA plates. Specimens BEM10L and BEM10H achieved a 19.6% and 29.4% increase in deflection at peak load, respectively, while BEM12L and BEM12H achieved a 22.4% and 33.6% increase, respectively. Therefore, the spacing between bolts influenced the ductility much more than the strength of the strengthened specimens. In addition, increasing the diameter, embedment depth, and torque magnitude of the EAB resulted in a slight increase in ductility when examining the deflection increase between BEM10H and BEM12H. This increase is more evident when observing the percentage deflection increase in specimens BM10H and BM12H, which were 14.3% and 40.6%.

The variation in EAB layout (i.e. spacing) was investigated to observe its impact on the beam's utilization of the AA plate during all stages of loading. In this study, two layouts were investigated: (a) EAB MF in series; (b) EAB MF at the ends of the AA plates. Both strength and ductility were affected in which BEM10E and BEM12E achieved a 28.9% and 34.1% increase in strength with a 4.25% and 46.9% increase in deflection, respectively. A slight increase in strength was reported between the aforementioned specimens, whereas significant increase in deflection and therefore ductility was observed. Therefore, using EAB with larger diameters, embedment depths, and torque magnitudes as end-anchors has proven to be more efficient than bolting throughout the composite plate. The reasons behind this can be attributed to: (a) rigid mechanical interlock between the EAB and inner concrete surface resulting in a stronger fixture; (b) larger AA plate length contribution at mid-span of the plate within the vicinity of the loading plates resulting in ideal stress distribution along the un-bolted length of the plate; (c) eliminating excessive slippage by combining large EAB with epoxy bonding.

3.2. Load-aluminum tensile strain response

The contribution of the composite action was monitored by plotting the load versus aluminum strain curves at mid-span of the tested specimens, as shown in Fig. 12. It is clearly indicated that most of the plated specimens, from both groups, actively engaged the AA plates and demonstrated yielding during peak load conditions. Similar to the load-deflection response, specimen CBE was plotted in both figures to serve as a benchmark in studying the effect of implementing mechanical fasteners to bonded/unbounded AA plates in the strengthened RC beams.

Furthermore, a pattern was observed related to the profile of each curve with respect to the unique characteristics in each specimen. For instance, the AA plates in most of the strengthened RC beams in M10 and M12 groups achieved higher strains than that of CBE, as shown in Fig. 12. Higher magnitudes of aluminum strains increase the curvature of the beam which in turn increases the stress concentration in the steel reinforcement and supplements the RC section with a larger moment capacity. Similar observations were reported by other researchers [33]. In Fig. 12(a), all beam specimens showed different strain values in the AA plate at the same load level. At 20 kN load, BEM10L and BM10H showed higher strain values while CBE and BEM10E showed lower strain values at the same load. At 40 kN and 60 kN loads, the difference in strain values in the AA plates among the tested beams increased with CBE and BEM12E that showed the largest strain values at these load levels. This trend continued until the load approached the ultimate load (80 kN) where the strain values in AA plates increased without a noticeable increase in the load signaling the yielding of AA plate. It is also observed from Fig. 12(a) that BEM10L showed the highest ultimate strain in AA plate compared to other beam specimens and therefore more utilization of the AA plate as an externally bonded strengthening material. Moreover, the specimen which consisted of the lowest number of M10-EAB, BEM10L, yielded a curve that overlapped that of CBE; meaning, that composite behavior of a strengthened specimen with a lower number of EAB imitated that of a strengthened specimen with only an EB AA plate. Due to the sufficient composite action induced by the large number of M10-EAB, Specimens BEM10H, BM10H, and BEM10E resisted larger loads at smaller strain values than those of specimens BEM10L and CBE; indicating a significant increase in the sections' stiffness. This observation is consistent with the load versus deflection

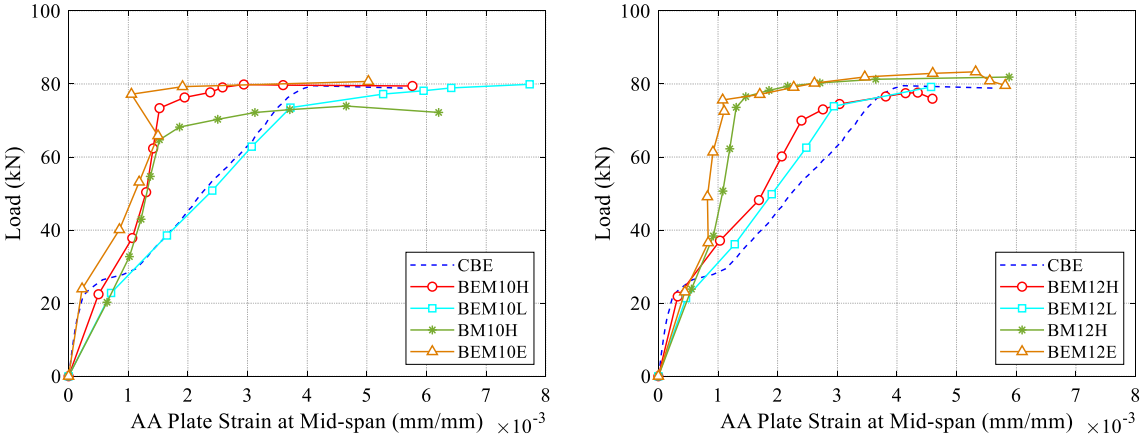

(a) CBE and M10 group of specimens.

(b) CBE and M12 group of specimens.

Fig. 12. Load versus aluminum strain curves for the strengthened RC specimens.

curve of specimen BM10H, shown in Fig. 10**(a)**, compared to the other curves for the specimens in the M10 group**.** In addition, the EAB layout affected the strengthened RC beam's composite behavior in which specimen BEM10E showed the highest load at the lowest aluminum strain measurement. Therefore, mechanical fasteners in the form of end-anchors allowed the RC beam to utilize more of the AA plate length during earlier stages of loading; thus, engaging the AA plate the most.

The strengthened RC beams in the M12 group of specimens, however, behaved differently during testing, as shown in Fig. 12**(b)**. All beam specimens showed very much the same strain values in the AA plate up to 25 kN. As the load increased, specifically at 40 kN, 60 kN and up to 70 kN, the strain at AA plate increased consistently where beam specimen CBE showed the highest strain value and beam specimen BEM12E showed the lowest strain value. This trend continued until the load approached the ultimate load where the strain values in AA plates increased without a noticeable increase in the load signaling the yielding of AA plate. Moreover, it is observed from Fig. 12(b) that almost all beam specimens failed at comparable ultimate strain values. This indicated that the increase in diameters, embedment depths, and torque magnitudes enhanced the composite behavior of the strengthened RC beams more than the specimens in the M10 group, which in turn allowed the MF specimens in the M12 group gain larger stiffness. For example, the curve of specimen BM12H, shown in Fig. 12**(b)**, achieved a larger stiffness again than that of specimen BM10H, shown in Fig. 12**(a)**. This phenomenon is attributed to the minimization of plate slip resulting from the tight fixture between the concrete and AA plate surfaces. Similar to the M10 group of specimens, the number of EAB affected the AA plate's contribution during testing where specimen BEM12L achieved its ultimate loading capacity at a larger aluminum strain than that of BEM12H. However, the strain readings in specimens BEM12L and BEM12H indicated lower aluminum strain than that of BM12H. This occurrence was the result of segmenting the stresses at different lengths of the AA plate using only M12-EAB, as in BM12H, rather than distributing the stresses along the entire plate using both M12-EAB and epoxy, as in BEM12H and BEM12L. Finally, BEM12E behaved similar to specimen BEM10E whereby the length in between the vicinity of the loading plates was strained due to the mechanical fasteners at the ends of the plate.

3.3. Load-concrete compressive strain response

Fig. 13 presents the load versus concrete compressive strain which is the result of a compressive stress acting on the top concrete layers of the section due to bending. These strain values were measured at mid-span for all the tested specimens in this study. It is worth mentioning that the strain gauge in specimen CB read until a value of 0.00230, after which it malfunctioned due to concrete spalling underneath it. Furthermore, all strengthened specimens reached concrete crushing strain of 0.003, which is defined as the crushing strain limit in concrete as per ACI 318-19 [25]. This indicates that all anchorage techniques have fully utilized the concrete area during all stages of loading. Additionally, since the large strain values measured in the AA plates induced additional stresses in the longitudinal steel reinforcement, the curvature of the beam was increased such that larger compressive strains were acting in the top layers of concrete.

It can be deduced that increasing the number of EAB in the strengthened RC beams, with bonded AA plates, resulted in increase in the slopes of the curves as shown in Fig. 13. Also, specimen BM10H exhibited the lowest load capacity compared to the other retrofitted RC beams in M10 group of specimens, as shown in Fig. 13**(a)**. This is consistent with the other figures described earlier. From Fig. 13**(b)** it is evident that increasing the EAB diameter, embedment depth, and torque magnitude unified the curves such that the presence or absence of adhesive bonding was not effective during testing.

3.4. Summary of load, deflection and strain

The results demonstrated in the previous figures were summarized and outlined in Table 6. In addition, the strain measurements at peak loads were used to study the type of behavior exhibited by specimens at ultimate loads. It is worth mentioning that strain gauge attached to the steel reinforcements in specimen BEM10L-2 malfunctioned during loading; hence, the abbreviation NA was used instead, as shown in Table 6. Specimen CB achieved an ultimate load of 64.2 kN at a concrete strain of 0.0023 mm/mm, which is when concrete exhibits its ultimate compressive strength. However, all the other specimens reached their ultimate loading capacities at concrete crushing, i.e., at concrete compressive strain value roughly greater than or equal to 0.003 mm/mm. All strengthened RC beams exhibited steel yielding (SY), aluminum yielding (AY), and concrete crushing (CC) at their peak loads. In addition, all the specimens in M10 and M12 groups reached deflection values greater than that of CBE, as shown in Table 6, which indicates substantial ductility for specimens anchored with EAB.

Fig. 14 shows a summary of the strength gains exhibited by each strenthened specimen with respect to CB. It is clearly indicated that the absence of pre-drilled holes granted CBE the capability of gaining strength relative to that of the other strengthened RC beams. In addition, the implementation of M12-EAB in the form of end-anchors allowed specimen BEM12E to exhibit the largest strength gain during testing. This phenomenon is the result of shifting the tensile stress concentration to the cross-sectional area of the plate without any holes—at the plate's mid-span. Furthermore, the increase in diameter, embedment depth,

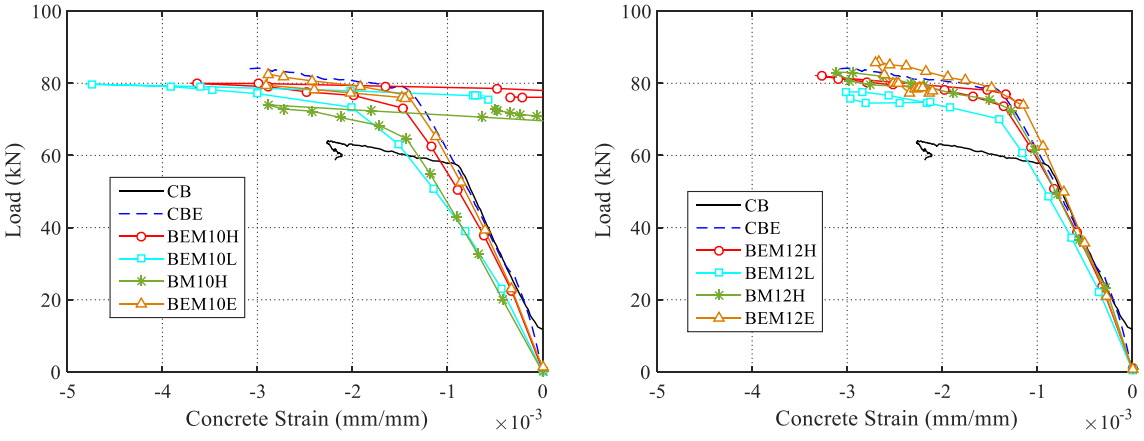

(a) CB, CBE and M10 group of specimens. (b) CB, CBE and M12 group of specimens.

Fig. 13. Load versus concrete compressive strain for all tested specimens.

Table 6
Summary of ultimate loads, deflections and strains for tested specimens.

Group	Specimen Designation	Ultimate[a]		Measured strain at ultimate load (mm/mm)		
		P_u (kN)	Δ_u (mm)	Concrete	Longitudinal reinforcement	AA plate
CBG	CB	64.2	17.4	0.0023	0.0136	–
	CBE	84.4	14.3	0.00301	0.00431	0.00495
M10	BEM10H-1	80.5	15.6	0.00403	0.00598	0.00623
	BEM10H-2	84.5	18.5	0.00358	0.00501	0.00695
	BEM10L-1	80	16	0.00303	NA	0.00701
	BEM10L-2	85.8	17.1	0.00298	0.00413	0.00803
	BM10H-1	74.4	16.4	0.00322	0.00596	0.00651
	BM10H-2	79.5	22	0.00298	0.00318	0.00224
	BEM10E	82.6	14.9	0.00308	0.00398	0.00676
M12	BEM12H-1	82.2	18.3	0.00326	0.00368	0.00584
	BEM12H-2	85.2	19.1	0.00299	0.00407	0.00586
	BEM12L-1	78.1	16.1	0.00298	0.00427	0.00484
	BEM12L-2	85.4	16.5	0.00367	0.00594	0.00649
	BM12H-1	83.5	19.5	0.00298	0.00587	0.00545
	BM12H-2	83.8	20.1	0.00365	0.00473	0.00424
	BEM12E	86.1	21	0.0037	0.00559	0.00593

[a] P_u = ultimate load; Δ_u = deflection at ultimate load.

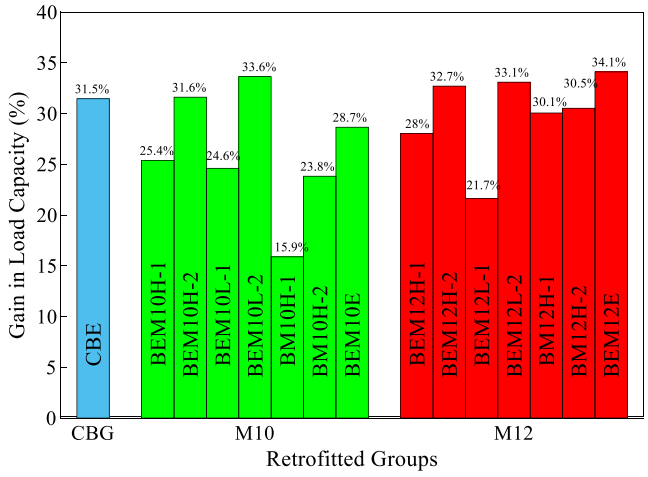

Fig. 14. Summary of strength gain in strengthened RC beams.

and torque magnitude allowed more than half of the retrofitted RC specimens in the M12-Specimens group to exhibit percentage strength gains greater than 30%. It is worth mentioning that since AA plates have relatively lower ultimate strengths than other strengthening composites, larger strength gains can be achieved by increasing the thickness of the plate or by using AA plate with higher strength.

3.5. Summary of ductility indices and failure modes

Other findings that were reported during this study were related to significant increase in ductility and the drastic shifts in premature failure modes. To quantify the ductility of each specimen, the ductility index at ultimate load (δ_u) and the ductility index at failure load (δ_f) were calculated using Eq. (1a) and (1b). Table 7 presents the deflections recorded at yielding (Δ_y), ultimate load (Δ_u), and failure (Δ_f) that were used to calculate the ductility indices, δ_u and δ_f, for all the tested specimens. The ductility index of specimen CBE was used as a benchmark to calculate the ductility gain exhibited by the specimens with EAB. This would provide insight on which EAB configuration improved the ductility of a conventional RC beam EB with an AA plate. The ratio of the ductility index for each specimen to that of CBE was calculated, as shown in Table 7. As a result, at peak load conditions, eleven out of fourteen of the strengthened RC beams MF with stronger composite materials, which impose large stress concentrations at the EAB locations, were not used. Furthermore, specimen CB exhibited a typical flexural failure, which is steel yielding (SY) followed by concrete crushing (CC), whereas specimen CBE exhibited SY followed by CC and end-plate debonding (ED). The specimens that were MF with bonded/un-bonded AA plates exhibited SY followed by CC and either local-plate

Table 7
Summary of ductility indices and failure modes for tested specimens.

Group	Specimen Designation	Deflection (mm)			Ductility Index		Ratio		Failure modes[a]
		Δ_y (mm)	Δ_u (mm)	Δ_f (mm)	δ_u	δ_f	$\delta_u/\delta_{u,CBE}$	$\delta_f/\delta_{f,CBE}$	
CBG	CB	6.77	17.4	30.5	2.57	4.51	–	–	CC, SY
	CBE	6.62	14.3	19.9	2.16	3.01	1	1	CC, SY, ED
M10	BEM10H-1	8.23	15.6	29.4	1.90	3.57	0.877	1.19	CC, SY, PR
	BEM10H-2	7.1	18.5	26.5	2.61	3.73	1.21	1.24	CC, SY, PR
	BEM10L-1	7	16	25	2.29	3.57	1.06	1.19	CC, SY, PR
	BEM10L-2	7.06	17.1	24.4	2.42	3.46	1.12	1.15	CC, SY, PR
	BM10H-1	6.9	16.4	32.7	2.38	4.74	1.10	1.57	CC, SY, PR
	BM10H-2	7.45	22	25.9	2.95	3.48	1.37	1.15	CC, SY, PR
	BEM10E	7.09	14.9	24.8	2.10	3.50	0.97	1.16	CC, SY, LD
M12	BEM12H-1	8.96	18.3	23.6	2.04	2.63	0.95	0.874	CC, SY, PR
	BEM12H-2	6.9	19.1	31.3	2.77	4.54	1.28	1.51	CC, SY, PR
	BEM12L-1	6.81	16.1	24.6	2.36	3.61	1.09	1.20	CC, SY, PR
	BEM12L-2	6.69	16.5	25	2.47	3.74	1.14	1.24	CC, SY, PR
	BM12H-1	7.17	19.5	26.1	2.72	3.64	1.26	1.21	CC, SY, PR
	BM12H-2	5.95	20.1	28.7	3.38	4.82	1.56	1.60	CC, SY, PR
	BEM12E	7.40	21	41	2.84	5.54	1.31	1.84	CC, SY, LD

[a] CC = concrete crushing; SY = steel yielding; PR = plate rupture; LD = local-plate debonding; ED = end-plate debonding.

debonding (LD) or plate rupture (PR). LD occurred in the specimens that were anchored at the ends of the plates, due to heavy plate-extension at mid-span of the specimen followed by buckling of the plate. The rest of the strengthened RC beams that were MF despite the spacing, type of EAB, or presence of adhesive exhibited PR. It is worth mentioning that a conventional RC beam (CB) yielded a ductility index that is greater than 60% (δf) and 73.3% (δu) of the tested specimens, which is expected since this is a conventional RC beam. However, one of the major objectives of this study was to evaluate the change in ductility of RC beams strengthened with MF plates (M10 and M12 specimens) compared to that of the control beam with EB plate (CBE).

$$\delta_u = \frac{\Delta_y}{\Delta_u} \tag{1a}$$

$$\delta_f = \frac{\Delta_y}{\Delta_f} \tag{1b}$$

Fig. 15 shows a summary of the ductility gains ehhibited by each strengthened RC beam over CBE at both ultimate and failure loading conditions. It can be observed that more than 75% of the strengthened RC beams using MF bonded/un-bonded AA plates demonstrated larger ductility gains than that of specimen CBE in both loading conditions. Furthermore, the most efficient specimen that actively engaged the ductility of the AA plate at ultimate load was specimen BM12H, as shown in Fig. 15**(a)**, whereas specimen BEM12E achieved the largest ductility gain at failure load, as shown in Fig. 15**(b)**. This indicated that the implementation of M12-EAB significantly influenced the ductility of the strengthened RC sections during testing due to the larger diameter,

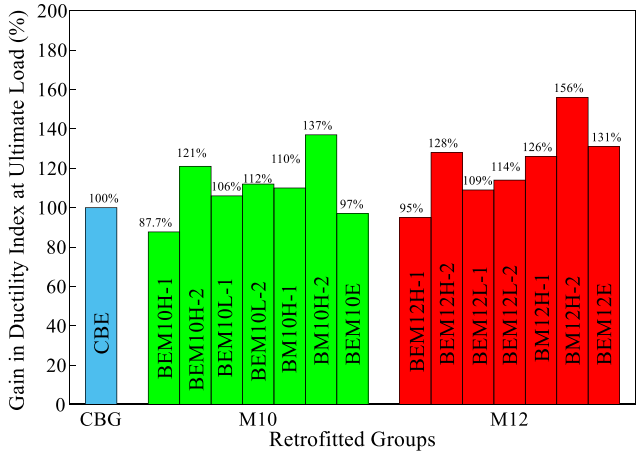

(a) Ductility index gain at ultimate loading.

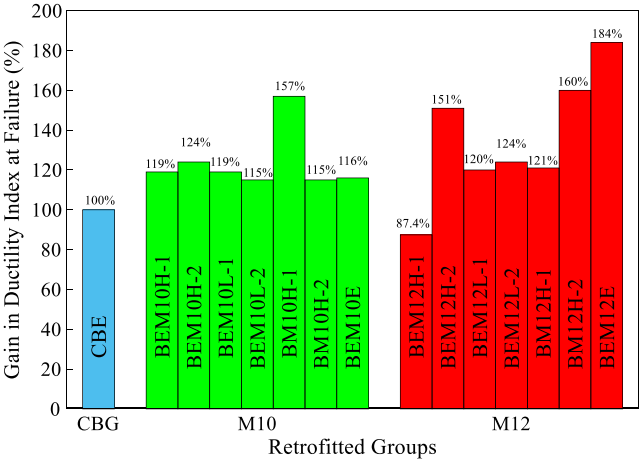

(a) Ductility index gain at failure load.

Fig. 15. Summary of ductility gain in strengthened RC beams.

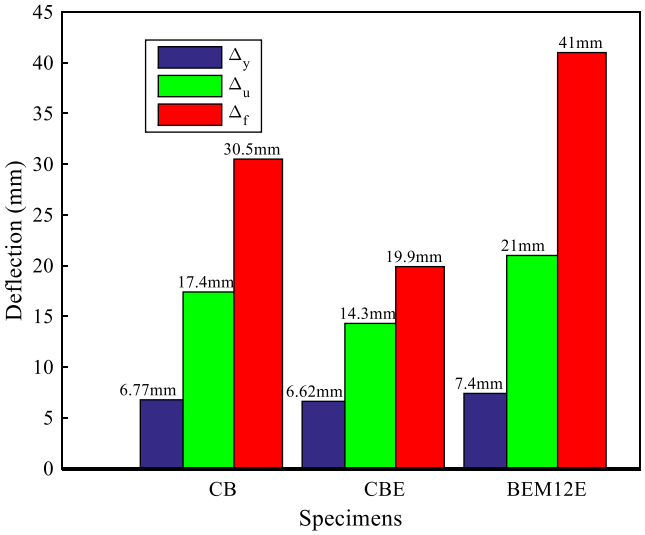

Fig. 16. Deflection at yield, ultimate, and failure load conditions for selected specimens.

embedment depth, and torque magnitude.

Fig. 16 shows the deflection at different loading conditions for specimens CB, CBE, and BEM12E. Due to sudden end-plate debonding failure, specimen CBE achieved a lower deflection than that of specimen CB, despite the large strength gain discussed in the previous sections. However, specimen BEM12E demonstrated the largest deformations at all loading conditions compared to both CB and CBE. This indicates that the combination of end EAB layout with larger EAB diameters, embedment depths, and torque magnitudes enhanced the flexural behavior, in terms of strength and ductility, of the RC beam.

4. Analytical predictions

The peak load capacities are numerically predicted using ACI 440.2R-17 [9] and ACI 318-19 [25]. By using the ACI 440.2R-17 guidelines the effect of debonding is accounted for such that the results will be conservative, while using ACI 318-19 indicates that the section is performing as a typical RC beam with an additional tensile force in the AA plate location, as shown in Fig. 17. The nominal flexural strength of strengthened RC beam specimens is calculated using Eq. (2) in accordance with the ACI 440.2R-17 [9] guidelines:

$$M_n = A_s f_y \left(d - \frac{\beta_1 c}{2}\right) + \psi_1 A_a f_{fe} \left(h - \frac{\beta_1 c}{2}\right) \tag{2}$$

Where A_s is the area of the longitudinal steel reinforcement bars (mm^2); fy is the steel yield strength (MPa); d is the depth of the section (mm) measured from the top compression fiber to the center of tensile steel reinforcement; β_1 is the depth of equivalent rectangular strength block to the depth of the neutral axis (a/c); c is the distance from top concrete

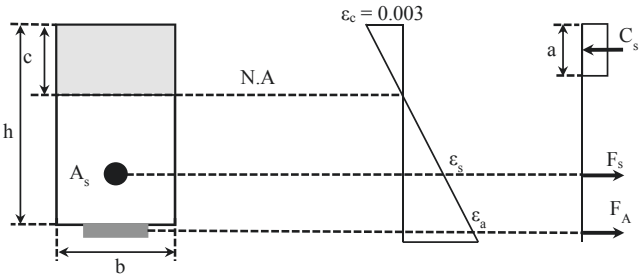

(a) Cross section of strengthened RC beam. (b) Stress and strain profiles.

Fig. 17. Stress and strain profiles in strengthened RC beam section at failure.

fiber to the neutral axis (mm); ψ_1 is FRP flexural strength reduction factor which was taken as 1 due to full composite action…; A_a is the area of the AA plates (mm^2); h is the beam's total height of cross-section (mm); and f_{fe} is the effective stress in the AA plates at failure and is calculated as follows:

$$f_{fe} = \varepsilon_{fe} E_f \tag{3}$$

$$\varepsilon_{fe} = \varepsilon_{cu}\left(\frac{d_f - c}{c}\right) - \varepsilon_{bi} \le \varepsilon_{fd} \tag{4}$$

Where ε_{fe} is the effective strain in the CFRP laminates at failure; ε_{cu} is the concrete crushing strain of 0.003; ε_{bi} is initial strain in the concrete substrate during AA plate installation, which was taken as zero since the specimens were not subjected to any kind of initial loads; ε_{fd} is the FRP debonding strain calculated as follows:

$$\varepsilon_{fd} = 0.41\sqrt{\frac{f'_{cc}}{nE_f t_f}} \le 0.9\varepsilon_{fu} \tag{5}$$

where f'_{cc} is the cylindrical compressive strength of concrete (MPa), which was taken as 0.8 multiplied by the average compressive strength of tested cubes; n is the number of AA plates used, which was taken as one; E_f is the elastic modulus of the AA plates, measured to be 70GPa; t_f is the thickness of the AA plates (mm); and ε_{fu} is the ultimate strain of the AA plates.

The ACI 318-19 guidelines were also followed to compute the nominal flexural strength of strengthened RC beam specimens using Eq. (6), where the equation almost resembles that of Eq. (2) but with the assumption that the AA plate has fully yielded at failure.

$$M_n = A_s f_y\left(d - \frac{\beta_1 c}{2}\right) + A_a f_{y,a}\left(h - \frac{\beta_1 c}{2}\right) \tag{6}$$

Where $f_{y,a}$ is the yield strength of aluminum and the rest of the parameters were defined in Eq (2).

Table 8 presents the percentage error between the numerical predictions compared to the experimental measurements taken during the test. It is observed that the flexural capacity model in ACI 318-19 outperformed that of ACI 440.R-17 in which most of the predictions of ACI 318-19 fell below 5% error, whereas the predictions made by ACI 440.R-17 reached up to 17.3% error.

A closer look at the results reveals that, unlike the design of a typically strengthened RC beam with EB composites, a strengthened RC beam with a MF-AA plate can be assumed to have a small or negligible slip when subjected to bending load. This assumption supports a strain compatible section, for the AA plate (i.e., plane section before bending remains plane after bending), such that the flexural capacity of the strengthened beam can be computed by simply taking the total of two lever arms from the internal longitudinal steel reinforcement and the AA plate, respectively. Therefore, the ACI 318-19 standards, which is typically used for RC beam designs, can be used instead of the more complicated and iterative approach prescribed in the ACI 440.R-17, which also contains multiple correction factors to account for premature failures.

Table 8
Analytical predictions based on ACI318-19 and ACI 440.2R-17 guidelines.

Group	Specimen Designation	Experiment	Predicted $(P_u)_{pred}$ (kN)		|% Error = $(1-(Pu)_{pred}/(Pu)_{exp})$|	
		$(P_u)_{exp}$ (kN)	*ACI 440.2R-17*	*ACI 318-19*	*ACI 440.2R-17*	*ACI 318-19*
CBG	CB	64.2	–	62.3	–	2.96
	CBE	84.4	71.2	81.5	15.6	3.44
M10	BEM10H-1	80.5	71.2	81.5	11.6	1.24
	BEM10H-2	84.5	71.2	81.5	15.7	3.55
	BEM10L-1	80	71.2	81.5	11.0	1.88
	BEM10L-2	85.8	71.2	81.5	17.0	5.01
	BM10H-1	74.4	71.2	81.5	4.30	9.54
	BM10H-2	79.5	71.2	81.5	10.4	2.52
	BEM10E	82.6	71.2	81.5	13.8	1.33
M12	BEM12H-1	82.2	71.2	81.5	13.4	0.85
	BEM12H-2	85.2	71.2	81.5	16.4	4.34
	BEM12L-1	78.1	71.2	81.5	8.83	4.35
	BEM12L-2	85.4	71.2	81.5	16.6	4.57
	BM12H-1	83.5	71.2	81.5	14.7	2.40
	BM12H-2	83.8	71.2	81.5	15.0	2.74
	BEM12E	86.1	71.2	81.5	17.3	5.34

5. Limitations and future works

Although this paper has thoroughly investigated the effects of mechanical fasteners on the flexural capacity, ductility, and failure modes of the AA plated RC specimens, there are other parameters that should be accounted for during testing. An increase in the cross-sectional area of the AA plate, for instance, would result in a higher load-carrying capacity. Such strengthened specimens would begin to exhibit variations in load-carrying capacity based on the number and size of holes present in the AA plate as well as on the other factors discussed in this paper. Therefore, the volumetric ratio of the AA plate and scale of the specimens should also be considered as important parameter in future investigations.

Furthermore, fixture criteria that are associated with the potential failure modes within EAB should be addressed in future tests. In this study, these fixture criteria were adopted from the manufacturer such that premature concrete failure modes that arise from the minimum center-to-center spacing between each EAB, the minimum distance between the EAB and edge of the beam, and torque required to fix the EAB were prevented.

The amount of internal reinforcement, in both the longitudinal and transverse directions, is also a factor that should be considered when designing the anchorage system. This is true for RC beams that are heavily reinforced with steel bars such that installing EAB will be difficult or even impossible due to the interference and obstruction that would occur between the EAB and steel bars. However, this can be mitigated by using a nondestructive toolkit, like an ultrasonic pulse velocity test, to potentially detect the presence of steel reinforcement with a certain degree of accuracy. The locations at which steel reinforcement is detected could then be marked to begin EAB installation. In general, due to the ease of fitting stirrups along the length of the beam rather than lining the longitudinal bars along the width of the beam, the longitudinal reinforcement will influence whether EAB can be installed or not. Such limitations should also be tackled in future investigations.

Since AA plates are manufactured in batches of sheets with constant lengths, another limitation of using it for strengthening applications would be on RC girders that are significantly long. This would require further study of and testing on splicing to investigate different splicing lengths and techniques that will resolve such issues in strengthening longer girders and develop sufficient anchorage systems.

6. Summary & conclusions

This paper presented an experimental framework that investigated the viability and effectiveness of using expansion anchors (EAB) to mechanically fasten (MF) bonded/un-bonded AA plates to the soffits of deficient RC beams in flexure. Emphasis has been made on the specimens' flexural behavior by studying their load-deflection and load-strain response plots, ductility index values, and failure modes. Several experimental parameters were considered; namely, bolt size, embedment depth, spacing, and torque magnitudes. Based on the results of this experimental investigation, the following observations and conclusions could be drawn:

- The mechanical interlock that exists between the EAB's sleeves and the inner surfaces of the pre-drilled concrete holes played an essential role in postponing or preventing premature failures that would otherwise occur in beams strengthened using only externally bonded composite systems.
- All AA plated RC beams exhibited an increase in strength that ranged between 15.9 and 34.7% compared to the un-strengthened RC beam, despite the type of anchorage system implemented.
- Increasing the number of EAB in the strengthened RC beams with bonded AA plates did not contribute much in increasing the strength for specimens BEM10L and BEM10H, however, it slightly increased the beam's stiffness.
- The specimen that did not consist of epoxy in the M10-Specimens group (BM10H-1) exhibited the lowest strength gain (15.4%) as opposed to the other strengthened specimens. The absence of epoxy combined with M10-EAB significantly reduced the stiffness of the MF composite systems in the M10 group during the initial stages of loading.
- The increase in EAB diameter, embedment depth, and torque magnitude enhanced the composite action such that the section's composite actions significantly increased in specimens BM12H more than that of specimens BM10H.
- The incorporation of EAB as end-anchors yielded the most efficient strengthening system among all strengthened RC sections. The approach of positioning the EAB on the plate's ends maintained the original cross-sectional area of the plate at mid-span and provided uniform tensile stress distribution in the unbolted length.
- All MF bonded/unbonded AA plated systems demonstrated steel yielding and aluminum yielding prior to failure. The presence of anchors allowed the strengthened RC sections to distribute the stresses between the plates and steel bars such that the beams gained larger curvatures which enhanced their flexural capacities and ductility indices.
- Analytical predictions made by the ACI 318-19 outperformed the predictions made by ACI 4402.R-17. The use of EAB postponed or eliminated premature failure modes such that the peak load of a MF-RC beam can be analytically predicted by assuming an additional lever arm ($A_a f_{y,a}$) in the flexural capacity model.

Future research work involving higher grades of aluminum alloy plates such as AA 7068 and AA 7075 need to be tested using MF anchorage systems to investigate other possible types of failure modes which involve EAB shear, pullout, and pryout failures. Furthermore, durability and resilience tests that involve MF AA plated systems subjected to harsh environments, high temperatures, and cyclic loading need to be evaluated to investigate the viability of MF-AA plated composite systems in real-life construction projects.

CRediT authorship contribution statement

Omar R. Abuodeh: Methodology, Formal analysis, Investigation, Data curation, Writing - original draft, Writing - review & editing, Visualization. **Jamal A. Abdalla:** Methodology, Investigation, Supervision, Writing - original draft, Writing - review & editing. **Rami A. Hawileh:** Methodology, Investigation, Supervision, Writing - original draft, Writing - review & editing.

Declaration of Competing Interest

None.

Acknowledgment

The support for the research presented in this paper had been provided by Riad Sadek Endowed Chair in Civil Engineering at the American University of Sharjah. The support is gratefully appreciated and acknowledged. The views and conclusions, expressed or implied, in this study are those of the authors and should not be interpreted as those of the donor or the institution.

References

[1] Civil+structural. Keys to Success: Structural Repair and Strengthening Techniques for Concrete Facilities. [Online]. Available: https://csengineermag.com/ [accessed: 15-May-2018].
[2] Salama ASD, Hawileh RA, Abdalla JA. Performance of externally strengthened RC beams with side-bonded CFRP sheets. Compos Struct 2019;212:281–90.
[3] Douier KA, Hawileh R, Abdalla JA. Behavior of RC Beams externally strengthened with Mortar bonded Steel Mesh. 2019 Advances in Science and Engineering Technology International Conferences (ASET) 2019:1–3.
[4] Hawileh RA, Rasheed HA, Abdalla JA, Al-Tamimi AK. Behavior of reinforced concrete beams strengthened with externally bonded hybrid fiber reinforced polymer systems. Mater Des Jan. 2014;53:972–82.
[5] Ali A, Abdalla J, Hawileh R, Galal K. CFRP Mechanical Anchorage for Externally Strengthened RC Beams under Flexure. Phys Proc 2014;55:10–6.
[6] Banjara NK, Ramanjaneyulu K. Investigations on behaviour of flexural deficient and CFRP strengthened reinforced concrete beams under static and fatigue loading. Constr Build Mater 2019;201:746–62.
[7] Hawileh RA, Nawaz W, Abdalla JA, Saqan EI. Effect of flexural CFRP sheets on shear resistance of reinforced concrete beams. Compos Struct 2015;122:468–76.
[8] Al-Tamimi AK, Hawileh RA, Abdalla JA, Rasheed HA. Effects of Ratio of CFRP Plate Length to Shear Span and End Anchorage on Flexural Behavior of SCC RC Beams. J Compos Constr Dec. 2011;15(6):908–19.
[9] ACI Committee 440. Guide for the Design and Construction of Externally Bonded FRP Systems for Strengthening Concrete Structures. Farmington Hills, Michigan (USA): American Concrete Institute;, 2017.
[10] Esfahani MR, Kianoush MR, Tajari AR. Flexural behaviour of reinforced concrete beams strengthened by CFRP sheets. Eng Struct 2007;29(10):2428–44.
[11] Rasheed HA, Abdalla J, Hawileh R, Al-Tamimi AK. Flexural behavior of reinforced concrete beams strengthened with externally bonded Aluminum Alloy plates. Eng Struct 2017;147:473–85.
[12] Hawileh RA, Nawaz W, Abdalla JA. Flexural behavior of reinforced concrete beams externally strengthened with Hardwire Steel-Fiber sheets. Constr Build Mater 2018;172:562–73.
[13] Franco N, Biscaia H, Chastre C. Experimental and numerical analyses of flexurally-strengthened concrete T-beams with stainless steel. Eng Struct 2018;172:981–96.
[14] Franco N, Chastre C, Biscaia H. Strengthening RC Beams Using Stainless Steel Continuous Reinforcement Embedded at Ends. J Struct Eng 2020;146:1–15.
[15] El-Maaddawy Tamer A. Mechanically Fastened Composites for Retrofitting Corrosion-Damaged Reinforced-Concrete Beams: Experimental Investigation. J Compos Constr 2014;18(2):4013041.
[16] Bank LC, Arora D. Analysis of RC beams strengthened with mechanically fastened FRP (MF-FRP) strips. Compos Struct 2007;79(2):180–91.
[17] Grelle SV, Sneed LH. Review of Anchorage Systems for Externally Bonded FRP Laminates. Int J Concr Struct Mater 2013;7(1):17–33.
[18] Binh PH, Riadh A-M. Prediction Models for Debonding Failure Loads of Carbon Fiber Reinforced Polymer Retrofitted Reinforced Concrete Beams. J Compos Constr Feb. 2006;10(1):48–59.
[19] Mirghani AM, Abdalla JA, Hawileh RA. Modeling and simulation of bond-slip behavior of Aluminum Alloy plates adhesively bonded to concrete. In: 2017 7th International Conference on Modeling, Simulation, and Applied Optimization (ICMSAO); 2017. p. 1–5.
[20] Abu-Obeidah A, Hawileh RA, Abdalla JA. Finite element analysis of strengthened RC beams in shear with aluminum plates. Comput Struct 2015;147:36–46.
[21] Abdalla JA, Abu-Obeidah AS, Hawileh RA, Rasheed HA. Shear strengthening of reinforced concrete beams using externally-bonded aluminum alloy plates: An experimental study. Constr Build Mater 2016;128:24–37.
[22] Abuodeh OR, AlRifai M, Hawileh RA, Abdalla JA. Finite Element Modelling of Aluminum Alloy Plated Beams. In: 8th International Conference on Modeling Simulation and Applied Optimization (ICMSAO'19); 2019. p. 1–5.
[23] Abdalla JA, Hraib FH, Hawileh RA, Mirghani AM. Experimental investigation of bond-slip behavior of aluminum plates adhesively bonded to concrete. J Adhes Sci Technol Jan. 2017;31(1):82–99.
[24] Lamanna AJ, Bank LC, Scott DW. Flexural Strengthening of Reinforced Concrete Beams by Mechanically Attaching Fiber-Reinforced Polymer Strips. J Compos Constr 2004;8(3):203–10.
[25] ACI Committee 318. Building Code Requirements for Structural Concrete and Commentary. Farmington Hills, Michigan (USA): American Concrete Institute; 2019.

[26] HILTI, "HST-3 EXPANSION ANCHOR,"; 2019. [Online]. Available: https://www.hilti.ae/c/CLS_FASTENER_7135/CLS_WEDGE_ANCHORS_7135/ [accessed: 04-Dec-2018].
[27] ASTM C109/C109M-16a, Standard Test Method for Compressive Strength of Hydraulic Cement Mortars (Using 2-in. or [50-mm] Cube Specimens). West Conshohocken, PA: ASTM International; 2016.
[28] ASTM A370-18. Standard Test Methods and Definitions for Mechanical Testing of Steel Products. West Conshohocken, PA: ASTM International; 2018.
[29] ASTM E8/E8M-16a. Standard Test Methods for Tension Testing of Metallic Materials. West Conshohocken, PA: ASTM International; 2018.
[30] aalco, "Aluminium Alloy - Commercial Alloy - 5083 - '0' - H111 Sheet and Plate," Parkway House, Unit 6 Parkway Industrial Estate, Wednesbury WS10 7WP; 2019.
[31] MAPEI. Mapei–adhesives, sealants, chemical products for building; 2019. [Online]. Available: https://www.mapei.com/ [accessed: 16-Jan-2019].
[32] A. C. 546, Concrete Repair Guide. Farmington Hills, Michigan (USA); 2008.
[33] El Maaddawy T, Soudki K. Strengthening of reinforced concrete slabs with mechanically-anchored unbonded FRP system. Constr Build Mater 2008;22(4):444–55.